Increased Quasi Stationarity and Persistence of Winter Ural Blocking and Eurasian Extreme Cold Events in Response to Arctic Warming. Part I: Insights from Observational Analyses

YAO YAO AND DEHAI LUO

Key Laboratory of Regional Climate-Environment for Temperate East Asia, Institute of Atmospheric Physics, Chinese Academy of Sciences, Beijing, China

AIGUO DAI

Department of Atmospheric and Environmental Sciences, University at Albany, State University of New York, Albany, New York, and National Center for Atmospheric Research, Boulder, Colorado

IAN SIMMONDS

School of Earth Sciences, University of Melbourne, Parkville, Victoria, Australia

(Manuscript received 30 March 2016, in final form 30 December 2016)

ABSTRACT

Part I of this study examines the relationship among winter cold anomalies over Eurasia, Ural blocking (UB), and the background conditions associated with Arctic warming over the Barents and Kara Seas (BKS) using reanalysis data. It is found that the intensity, persistence, and occurrence region of UB-related Eurasian cold anomalies depend strongly on the strength and vertical shear (VS) of the mean westerly wind (MWW) over mid–high-latitude Eurasia related to BKS warming.

Observational analysis reveals that during 1951–2015 UB days are 64% (54%) more frequent during weak MWW (VS) winters, with 26.9 (28.4) days per winter, than during strong MWW (VS) winters. During weak MWW or VS winters, as frequently observed during 2000–15, persistent and large UB-related warming is seen over the BKS together with large and widespread midlatitude Eurasian cold anomalies resulting from increased quasi stationarity and persistence of the UB. By contrast, when the MWW or VS is strong as frequently observed during 1979–99, the cold anomaly is less intense and persistent and confined to a narrow region of Europe because of a rapid westward movement of the strong UB. For this case, the BKS warming is relatively weak and less persistent. The midlatitude cold anomalies are maintained primarily by reduced downward infrared radiation (IR), while the surface heat fluxes, IR, and advection all contribute to the BKS warming. Thus, the large BKS warming since 2000 weakens the meridional temperature gradient, MWW, and VS, which increases quasi stationarity and persistence of the UB (rather than its amplitude) and then leads to more widespread Eurasian cold events and further enhances the BKS warming.

1. Introduction

The frequent outbreak of extreme cold events during recent decades has been linked to the marked decrease of Arctic sea ice extent (SIE) in summer, autumn, and winter (Honda et al. 2009; Petoukhov and Semenov 2010; Overland et al. 2011; Liu et al. 2012; Outten and Esau 2012; Screen and Simmonds 2013a,b). However, the physical mechanism of how the Arctic sea ice reduction affects midlatitude extreme cold weather has been much debated, and it is still not fully understood (Francis and Vavrus 2012, 2015; Cohen et al. 2014; Mori et al. 2014; Tang et al. 2013; Vihma 2014; Walsh 2014; Simmonds and Govekar 2014: Kug et al. 2015; Gao et al. 2015).

Honda et al. (2009) noted that anomalous turbulent heat fluxes associated with the Arctic sea ice reduction over the Barents and Kara Seas (BKS) generate a stationary wave train that tends to amplify the Siberian high, thus causing cold winters over the Far East. Inoue et al. (2012) found that a northward shift of cyclone paths can create an anticyclonic circulation over the

Corresponding author e-mail: Dr. Dehai Luo, ldh@mail.iap.ac.cn

DOI: 10.1175/JCLI-D-16-0261.1

northern Siberian sector, resulting in cold Siberian anomalies. Newson (1973), Murray and Simmonds (1995), Liu et al. (2012), and Francis and Vavrus (2012, 2015) concluded that a decrease in zonal wind speeds could occur as a consequence of Arctic warming through the thermal wind equation, which could lead to increased atmospheric blocking and thus more extreme cold events. Screen and Simmonds (2013a,b) found that Arctic sea ice reduction can amplify planetary waves to generate extreme weather. More recently, Walsh (2014) pointed out that as the zonal wind speed weakens, the north–south meanders of the westerly jet stream can become so prominent that southward intrusions of polar cold air into the midlatitudes and northward intrusions of warmer air into higher latitudes might be enhanced. Such a meandering jet stream corresponds essentially to a blocking flow comprising several isolated anticyclones and cyclones, as first demonstrated by Luo (2000) in a two-layer model.

Although previous studies have suggested that the Arctic warming can amplify atmospheric planetary waves such as the blocking flows and retard their eastward propagation to favor extreme cold events (Newson 1973; Francis and Vavrus 2012, 2015; Screen and Simmonds 2013a,b; Cohen et al. 2014; Walsh 2014), how the amplified planetary waves affect the intensity, persistence, and occurrence region of winter cold anomalies is still unclear. More recently, Luo et al. (2016a,b) indicated that Ural blocking (UB) as a response to the winter Arctic sea ice loss over the BKS tends to be more long lived during 2000–13 than during 1979–99. In particular, the UB frequency shows an upward trend and is more frequent in the high latitudes than in the midlatitudes, although the blocking frequency over the whole of Eurasia does not show a clear trend. Such a long-lived UB pattern could lead to a strong dipole temperature anomaly with high-latitude warming and midlatitude cooling to amplify the warm Arctic–cold Eurasian (WACE) pattern. However, it is still unclear which atmospheric conditions in Eurasia affect the intensity, persistence, and occurrence region of midlatitude cold anomalies associated with the UB. This is one of the focuses of this study. As demonstrated by Luo (2000), the duration and position of meandering blocking depend strongly on the strength and vertical shear (VS) of the mean westerly wind (MWW). Thus, UB events can be classified in terms of the strengths of MWW and VS to examine the impact of different atmospheric conditions on cold anomalies associated with the UB related to Arctic warming, even though Screen and Francis (2016) noted that on longer time scales the phase of the Pacific decadal oscillation (PDO) can also modulate the atmospheric response to the Arctic sea ice loss.

In this paper, we quantify the impact of atmospheric background conditions (represented by MWW and VS) on winter Eurasian cold anomalies associated with the UB, while the atmospheric conditions are further linked to Arctic warming over the BKS. In Luo et al. (2017, hereafter Part II), we will perform a theoretical investigation to address the question of how the persistence and movement of a blocking flow are linked to the atmospheric conditions.

This paper is organized as follows. In section 2, we describe the data and methodology. Section 3 discusses the likely association among the weakening of the MWW and VS, the Arctic warming, the sea ice loss over the BKS, and the UB pattern. In section 4, we present the results on the relationship between Eurasian cold anomalies and the different movements and persistence of the UB patterns. The intensity, persistence, and occurrence area of winter cold and warm extremes and their link to the movement, persistence, and amplitude of UB patterns are examined in section 5. Conclusions and further discussion are presented in section 6.

2. Data and methodology

a. *Data and analysis procedures*

We use the monthly mean SIE data from NOAA National Snow and Ice Data Center (NSIDC; https://nsidc.org/) during wintertime [December–February (DJF)] from December 1978 to February 2015 (1979–2015 hereafter). We filled in the missing data by linear interpolation between the anomalies of November 1987 and February 1988 following Simmonds (2015). We also used the National Centers for Environmental Prediction (NCEP)–National Center for Atmospheric Research (NCAR) reanalysis daily data on a 2.5° × 2.5° grid for DJF 500-hPa geopotential height, multilevel winds, surface downward longwave radiation, latent and sensible heat fluxes, and surface air temperature (SAT) for the period from December 1950 to February 2015 (1951–2015 hereafter) (http://www.esrl.noaa.gov/psd/data/gridded/data.ncep.reanalysis.html).

The anomalies at each grid point during 1979–2015 or 1951–2015 were calculated as the deviation from their long-term (1979–2015 or 1951–2015) mean for each day of the winter. UB events in winter during 1951–2015 are classified in terms of the strengths of the MWW and VS to examine how the UB patterns and associated cold anomalies depend on the background conditions. We excluded the days with a UB event in deriving the winter background conditions, (i.e., we used the average over the winter days without the UB as the background value). For example, to separate the warming induced by UB from that induced by other factors over the BKS region

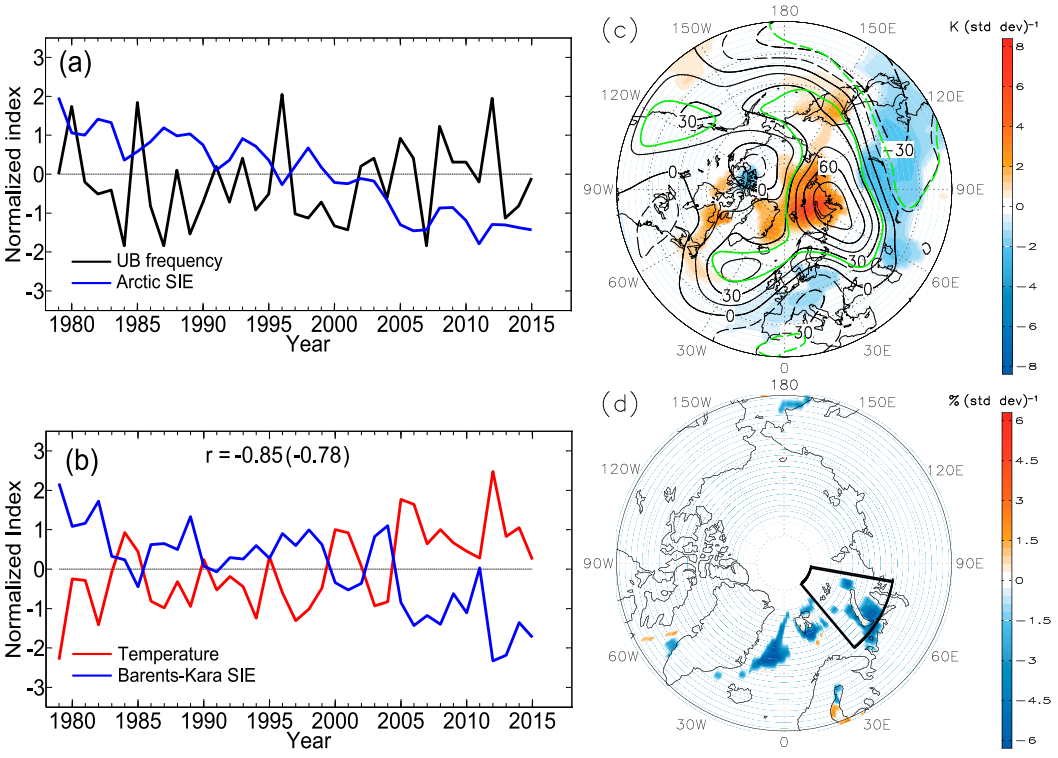

FIG. 1. (a) Time series of normalized winter Arctic SIE (blue line) and UB days (black line) from 1979 to 2015 and (b) time series of the normalized Barents and Kara SIE (blue line) and surface air temperature anomaly (red line) over the BKS region in winter (DJF) during 1979–2015. The correlation coefficient r between the two lines is given for the case with (and without) trends. (c) Linear regression map (north of 30°N) of DJF-mean 500-hPa height [contours; interval = 15 gpm (std dev)$^{-1}$] and SAT [color shading; K (std dev)$^{-1}$] anomaly fields projected onto the Arctic SIE time series [blue line in (a), multiplied by −1] with all the data being detrended prior to the regression. The green line encircles the area over which the regression coefficients are above the 95% confidence level based on the two-sided Student's t test. (d) Linear regression map (north of 60°N) of the DJF SIE onto the time series of the DJF UB frequency [black line in (a)] after detrending; the BKS region is shown by the black outlined area (70°–85°N, 40°–80°E). In (c) and (d), only the areas over which the SAT and SIE anomalies are above the 95% confidence level are plotted. The NCEP–NCAR reanalysis upper-air data were used in this and other figures.

(70°–85°N, 40°–80°E; see the black box in Fig. 1d), we calculated the SAT anomaly averaged over the winter days without UB for the BKS region $\overline{T}_{\mathrm{BSK}}$, which may be considered as a measure of background Arctic warming.

To calculate VS, we first define upper (lower) tropospheric mean zonal wind U_U (U_L) averaged over the winter days without UB as the vertically averaged MWW between 200 and 400 hPa (600 and 850 hPa) (cf. Fig. 2c). Then we define VS = $U_U - U_L$ at each grid box. To further quantify the connection between the variations of the winter MWW or VS and the background Arctic warming, we define the values of U_U and U_L averaged over the region (50°–75°N, 30°–90°E) (referred to as the UB region hereafter) as the upper and lower mean zonal winds U_{UA} and U_{LA}, respectively. We choose 50°–75°N, 30°–90°E because the UB events occur mainly in this region (Diao et al. 2006). We then define $\mathrm{VS}_A = U_{\mathrm{UA}} - U_{\mathrm{LA}}$ as the strength of the winter VS in the blocking region and use it as a measure of the background baroclinicity over the Ural region. In addition, the DJF-mean 300-hPa zonal wind without UB days averaged over the UB region $U_{300\mathrm{A}}$ is used as a measure of the strength of the regionally averaged MWW in the UB region. To examine the link between $U_{300\mathrm{A}}$ or VS_A and the background Arctic warming, we define DT = $\Delta T_S - \Delta T_N$ as the background meridional temperature gradient (MTG) over Eurasia similar to Luo et al. (2016a), where ΔT_S and ΔT_N denote the DJF-mean SAT anomalies (with UB days excluded) averaged over the midlatitude Eurasia (40°–60°N, 50°–90°E) and subarctic region (60°–85°N, 40°–80°E), respectively. Similar results are found if the BKS is defined as the subarctic region (not shown).

In this study, a Monte Carlo test is used to quantify the statistical significance for the difference of the mean duration or the temperature distribution between weak and strong VS (MWW) events. For example, for the VS (61 blocking cases with 20 UB events for the strong VS

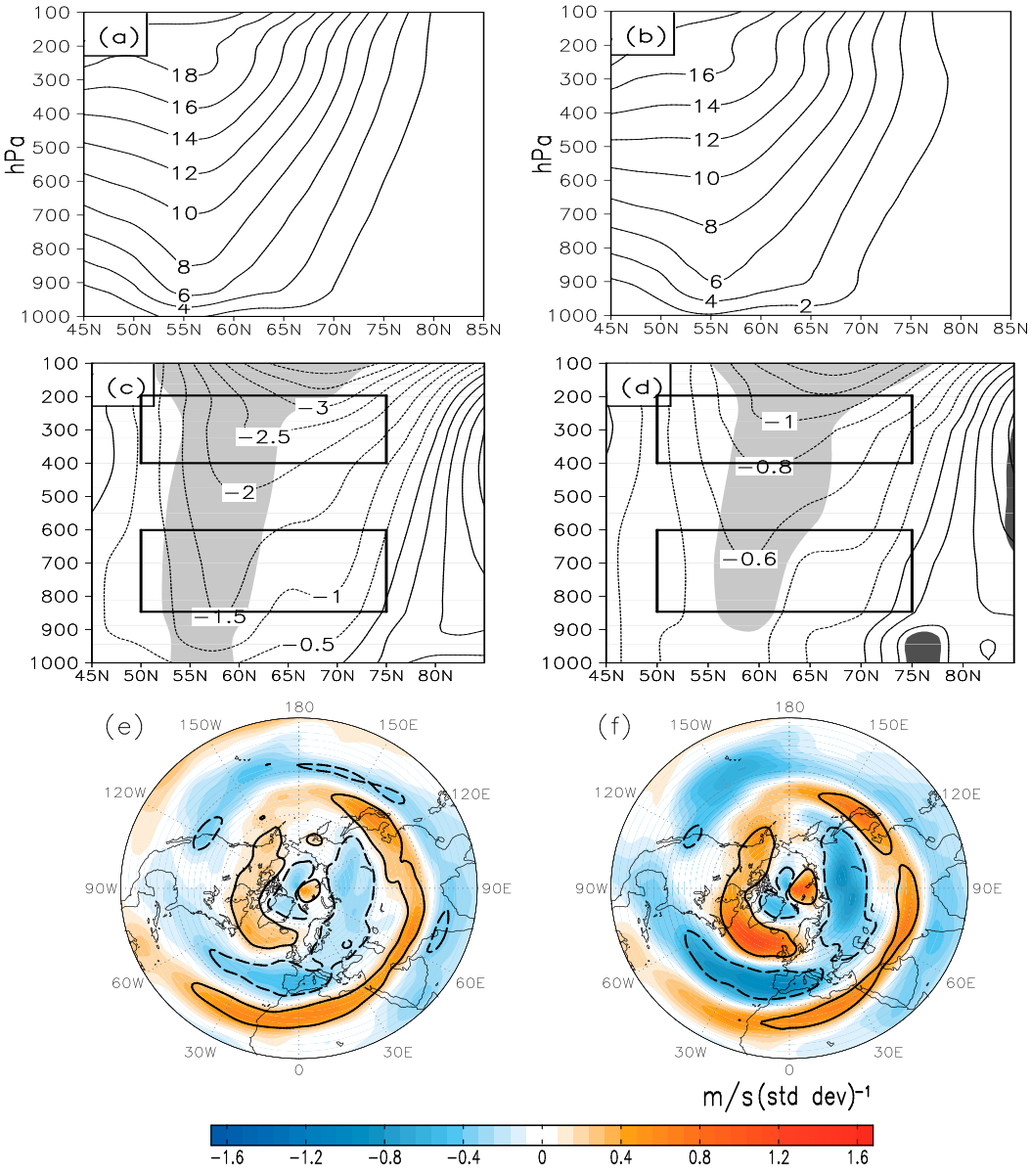

FIG. 2. Zonally averaged DJF-mean zonal winds (m s^{-1}) over the region 30°–90°E with UB events being excluded during (a) P1 and (b) P2 and (c) the P2 − P1 difference; (d) as in (c), but for geostrophic zonal wind derived from the thermal wind equation and background temperature fields for P1 and P2; and (e),(f) regression fields (north of 10°N) of DJF vertical shear [m s^{-1} (std dev)$^{-1}$] and 300-hPa zonal wind [m s^{-1} (std dev)$^{-1}$], respectively, into the detrended background Arctic warming time series $\overline{T}_{\mathrm{BSK}}$ during 1979–2015. In (c) and (d), the shading denotes the region above the 95% confidence level based on the two-sided Student's *t* test, whereas the rectangular boxes denote the two regions used to define the vertical shear of the mean zonal wind between the two upper and lower layers. In (e),(f), the solid and dashed contours encircle the region above the 95% confidence level based on the two-sided Student's *t* test.

and 41 UB events for the weak VS, as described below), 20 and 41 UB events are randomly chosen as two groups. Then, the mean durations are calculated for the two groups. A distribution of 1000 differences in duration can be given by performing the test 1000 times. On this basis, the level of statistical significance can be determined by examining where the difference of the duration between strong and weak VS events fits within the duration distribution. A similar significance test can be made for the temperature distribution below.

b. *Blocking detection method*

Here we used the one-dimensional blocking index of Tibaldi and Molteni (1990, hereafter TM) to identify the

UB events, as used by Luo et al. (2016a,b). This index is defined in terms of the 500-hPa geopotential height Z difference between three latitudes $\phi_n = 80°\text{N} + \Delta$, $\phi_o = 60°\text{N} + \Delta$, and $\phi_s = 40°\text{N} + \Delta$, at a given longitude λ and based on the criteria of GHGS $= [Z(\phi_0) - Z(\phi_s)]/(\phi_0 - \phi_s) > 0$ and GHGN $= [Z(\phi_n) - Z(\phi_0)]/(\phi_n - \phi_0) < -10\,\text{m}\,(°\,\text{lat})^{-1}$, where GHGS and GHGN denote the 500-hPa Z gradients in the lower- and higher-latitude regions for each given longitude, respectively. Note that $\Delta = -5°$, 0°, 5° were used here, as opposed to the −4°, 0°, 4° employed by TM. A 5-day moving average was applied to smooth out the synoptic noise of the daily 500-hPa Z anomalies prior to calculating the blocking index, so that the TM index reflects mostly the large-scale structure of blocking, as done by the NOAA Climate Prediction Center (CPC) (http://www.cpc.ncep.noaa.gov/products/precip/CWlink/blocking/index/index.nh.shtml). Such a treatment was widely applied in calculating the TM index of blocking events. A blocking event is said to have occurred if the above criteria are satisfied for at least three consecutive days. The period and strength of a blocking event can be calculated according to the definition on the NOAA CPC website. The calculation domain of the TM index covers the region from 30° to 90°E because the mean position of UB events is centered around 60°E (Diao et al. 2006).

3. The link of the mean westerly wind and its vertical shear with Arctic warming

a. *Links among Ural blocking, Arctic warming, and Arctic sea ice loss*

Although previous studies have revealed that the Arctic warming corresponds to a UB pattern (Luo et al. 2016a), the results presented below show a complex relationship between the Arctic sea ice loss, Arctic warming, and UB pattern. Figure 1a shows that the overall Arctic winter SIE undergoes a marked downward trend from 1979 to 2015, especially after 2000, as noticed previously (e.g., Simmonds 2015). Winter SIE over the BKS also shows large decreases, mostly from 1979 to 1985 and after 2004 (Fig. 1b). At the same time, a warming pattern is seen over the BKS region from 1979 to 2015, and hence there is a strong negative correlation between the BKS SIE and SAT (Fig. 1b). Figure 1c shows that large surface warming over the BKS region corresponds to a strong anticyclonic anomaly over the north side of the Ural Mountains, while a weak negative height anomaly emerges over the south of the Ural region. Such an anticyclonic circulation is referred to as the UB pattern hereafter, although its center differs slightly for different blocking events. Figure 1d further shows that an increased UB frequency corresponds to an SIE decline over the BKS and its adjacent region for year-to-year variations. Thus, Figs. 1c,d imply that the recent Arctic sea ice loss might be associated with an increased UB frequency and Arctic warming over the BKS. This indicates that the UB pattern, Arctic warming, and Arctic SIE variability and trends are strongly coupled with each other.

While there is a strong negative correlation of −0.85 (−0.78) between the BKS SIE and SAT with (without) trends, the correlation between the UB frequency and BKS SIE is not significant (correlation of −0.19 for both cases with and without trends), and the UB frequency shows only a weak trend (Fig. 1a). This can be explained in that the SIE variations are not only related to the changes in large-scale atmospheric circulations (Fang and Wallace 1994) but also related to changes in surface sea temperatures (SSTs) over the Arctic (Francis and Hunter 2007; Walsh 2014). In fact, the SIE variations may affect the UB pattern through the reduced meridional temperature gradient over Eurasia due to the Arctic warming over the BKS, as noted below. The UB frequency exhibits a positive correlation of 0.29 (0.27) with the SAT anomaly over the BKS during 2000–15 for a nondetrended (detrended) case because the Arctic warming (positive SAT anomaly) over the BKS is more prominent during 2000–15 (P2) than during 1979–99 (P1). Thus, the variations in UB frequency may be related to the Arctic warming over the BKS through changes in MWW and VS. Here our focus is on exploring how UB affects Eurasian cold events and how atmospheric background conditions associated with Arctic warming influence UB and thus the cold events. In this investigation, we do not examine the causal relationship between the UB frequency and Arctic sea ice loss.

b. *Mean westerly wind and its vertical shear and their link with Arctic warming*

As revealed in Fig. 1b, the BKS warming is more prominent during P2 than the earlier P1. Thus, it is helpful to examine the changes in MWW and VS from P1 to P2. Figures 2a–c show the latitude–pressure cross sections for zonally averaged DJF background zonal wind U (i.e., with UB events being excluded) averaged over the region 30°–90°E during these periods and their difference (P2 − P1). There is a clear reduction of the MWW in mid-to-high latitudes from P1 to P2, this being most pronounced in the upper troposphere (Fig. 2c). As shown by Screen and Simmonds (2010), amplified Arctic warming extends to the mid-to-upper troposphere. Such a warming pattern would lead to a reduction in meridional temperature gradients and thus weaken westerly winds and the vertical shear. The weakening of

the mid–high-latitude MWW and its vertical shear are consistent with the enhanced BKS warming during P2. This is made readily apparent by the P2 − P1 difference (Fig. 2d) of the geostrophic zonal wind derived from the background temperature fields $\overline{T}$ (i.e., with UB events being excluded) for P1 and P2 using the thermal wind equation as described in the appendix. Thus, we concluded that the recent warming over the BKS weakens MWW and VS and makes the background state over the Ural Mountains more barotropic.

Figures 2e,f show the regression patterns of the DJF VS and 300-hPa (the jet location) zonal wind U_{300} against the time series of the detrended $\overline{T}_{\mathrm{BSK}}$ (the mean SAT over the BKS with the UB days excluded; shown in Fig. 3a). It is seen that the VS and U_{300} decrease over mid–high-latitude Eurasia as $\overline{T}_{\mathrm{BSK}}$ increases (while increases are observed over the Atlantic and Pacific subtropics). This implies that the weakening of the MWW and VS over mid–high-latitude Eurasia is associated with the background Arctic warming. A similar feature is found at the 500-hPa level (not shown). Although Luo et al. (2016a) mentioned that the weakening of the MWW is probably due to Arctic warming, a detailed analysis on the link between them has not been done in previous studies.

As described in the appendix, a strong VS corresponds to a strong U_{300}, However, a strong U_{300} does not necessarily correspond to a strong VS if the meridional temperature gradient in the lower troposphere is strong. It is for this reason that it is of value to examine the correlation between U_{300} and VS as well as their difference in response to background Arctic warming over the BKS. Figure 3a compares the time series of the normalized nondetrended $\overline{T}_{\mathrm{BSK}}$ and background MTG over Eurasia during 1979–2015, while the normalized U_{300} and VS time series for the UB region during 1951–2015 are shown in Fig. 3b. The time series of the normalized winter UB days (frequency) and mean duration are shown in Fig. 3c during 1951–2015. The MTG (dashed line in Fig. 3a) exhibits a strong negative correlation of −0.94 (−0.91) with $\overline{T}_{\mathrm{BSK}}$ (solid in Fig. 3a) during 1979–2015 for the nondetrended (detrended) case. Such a high negative correlation is also found in both P1 and P2. This indicates that the background BKS warming reduces MTG over Eurasia. Figure 3 shows that the MWW has a positive correlation of 0.76 or 0.72 (0.76 or 0.66) with VS over the UB region during 1951–2015 or 1979–2015 for the nondetrended (detrended) case, which are statistically significant. Moreover, the VS exhibits a positive correlation of 0.77 or 0.8 (0.8 or 0.74) with the MTG during 1951–2015 or 1979–2015 for a nondetrended (detrended) case, while the MWW has a positive correlation of 0.64 or 0.70 (0.67 or 0.64) with the

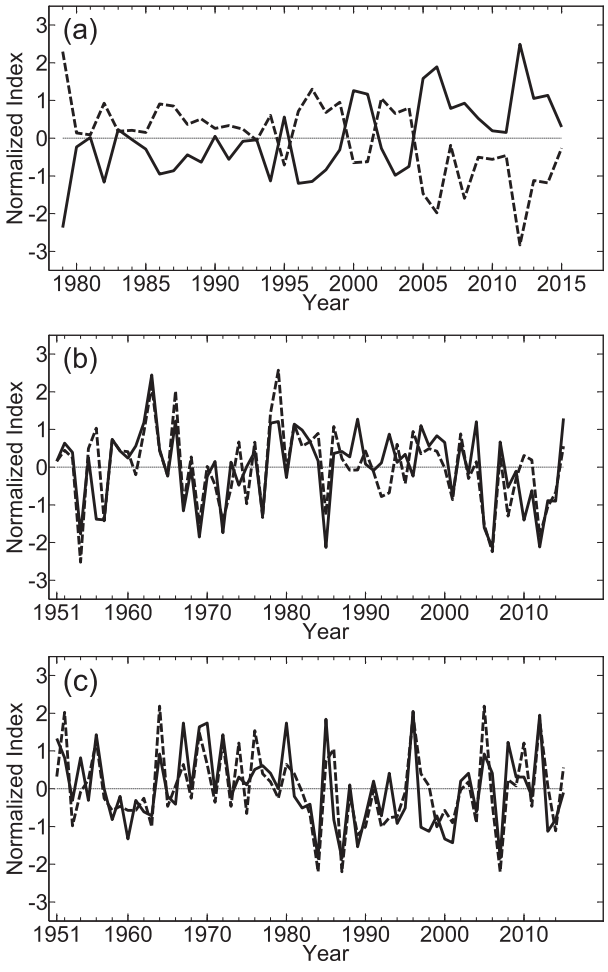

FIG. 3. Normalized (a) time series from 1979–2015 of the DJF-mean SAT anomaly $\overline{T}_{\mathrm{BSK}}$ (solid) averaged over the BKS region (70°–85°N, 40°–80°E), and the surface meridional temperature gradient (DT; dashed) between 40°–60°N, 50°–90°E and 60°–85°N, 40°–80°E with UB events being excluded. (b) Time series from 1951 to 2015 of the regionally averaged 300-hPa zonal wind (solid) over the region 50°–75°N, 30°–90°E and the vertical shear (dashed) of the zonal wind between the upper (400–200 hPa) and lower (850–600 hPa) layers averaged over 50°–75°N, 30°–90°E with UB events being excluded. (c) Time series of the UB days (solid) and mean duration (dashed) during 1951–2015.

MTG. In particular, the negative correlation of the MWW with the background BKS warming changes from −0.22 (−0.32) during P1 to −0.65 (−0.63) during P2 for a nondetrended (detrended) case, while the VS exhibits a negative correlation of −0.6 (−0.56) during P1 and −0.75 (−0.75) during P2 with the background BKS warming. It follows that the reduced MTG, and thus weak MWW and VS over Eurasia as observed during P2 (representing a more barotropic state), is associated with the enhanced background Arctic warming, although the warming trend has only a small contribution to their correlations. It can also be seen in Fig. 3b

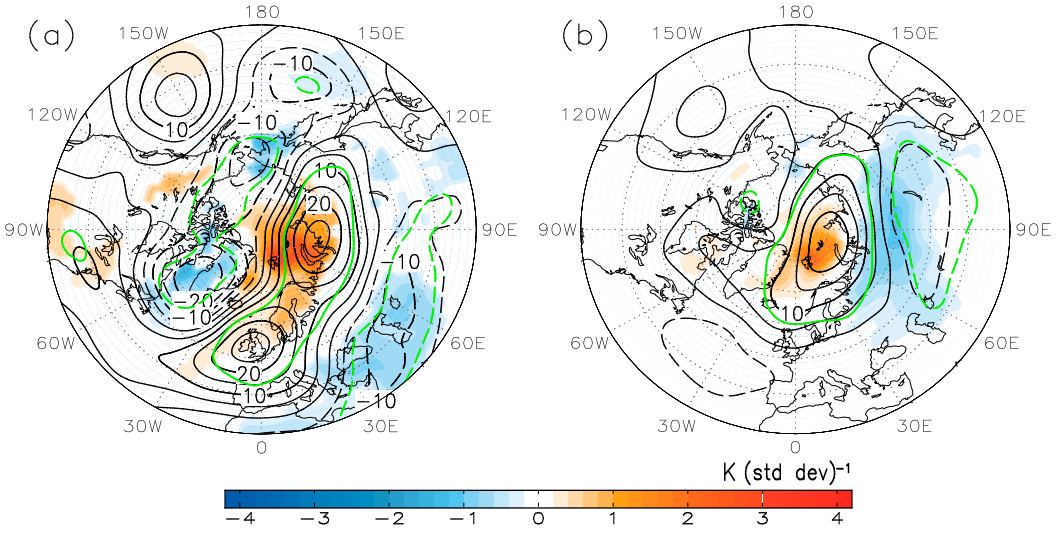

FIG. 4. Linear regression maps (north of 30°N) of DJF-mean 500-hPa height [contours; interval = 5 gpm (std dev)$^{-1}$] and SAT (color shading; only for areas above the 95% confidence level) anomaly fields projected onto the time series of the normalized (a) VS and (b) MWW over the UB region (50°–75°N, 30°–90°E) during 1951–2015 with trends being removed. The solid and dashed green contours denote the region above the 95% confidence level for the two-sided Student's *t* test.

that there are weak MWW and VS in the 1970s or 1950s. Actually, the weak MWW or VS in the 1950s is linked to the BKS warming associated with the sea ice decline there, which can be clearly seen from the detrended DJF-mean SAT anomaly (see Fig. 10b, red line). But the low MWW or VS in the 1970s is more likely related to the Eurasian cold anomaly (Cohen et al. 2014), as seen (see Fig. 10b, blue line).

The correlation analysis (Fig. 3c) reveals that while the UB days and mean duration have a positive correlation of 0.76 for (both) nondetrended and detrended cases, the UB days exhibit negative correlations of −0.53 and −0.32 (−0.56 and −0.37) with U_{300A} and VS_A that are statistically significant at the 99% confidence level. This indicates that the days of the UB tend to increase as the MWW or VS is reduced. While the negative correlation (−0.11) of the UB mean duration with the vertical shear VS_A is insignificant, its negative correlation (−0.38) with the MWW strength U_{300A} is statistically significant ($p < 0.01$). Thus, the UB mean duration is more sensitive to the strength of the MWW, although the UB days in winter are influenced by both the MWW and VS.

Figure 4 shows that when the MWW or VS is weak over the UB region, an anticyclonic anomaly circulation appears over the Ural Mountains and BKS region. From these regressed circulation fields, it can be deduced from advective processes that cold anomalies could appear mainly over southeastern Europe and central Asia for a weak VS (weak baroclinicity) case (Fig. 4a), while such cold anomalies might be seen mainly over central and East Asia for a weak MWW (Fig. 4b). Thus, the responses of height and temperature anomalies to the reduced MWW and VS strengths are slightly different because there is not a one-to-one correspondence between the weak MWW and VS strengths (Fig. 3b). As shown by Luo et al. (2016a), the winter UB frequency exhibits an increasing trend since about 2000 (cf. Fig. 1a) owing to decreasing zonal winds over Eurasia. Thus, the weakening trends of the MWW and VS since 2000 (Fig. 3b) would be expected to correspond to an enhanced anticyclonic circulation or more blocking over the Ural Mountains, which would lead to a cooling trend over central Asia and a warming trend over high-latitude Eurasia (discussed below). Thus, the WACE pattern (Luo et al. 2016a) would be enhanced during 2000–15. However, it is unclear how the daily evolutions of the UB pattern and the associated SAT anomalies depend on the strengths of MWW and VS. This is examined in the next section.

4. The link between Eurasian temperature anomalies and the strengths of mean westerly wind and its vertical shear

a. The frequency and duration of UB events

As revealed above, the BKS warming corresponds to a weakening MWW or VS. Here we quantify the impact of MWW and VS strengths on the UB. We approach this by comparing the winters with strong and

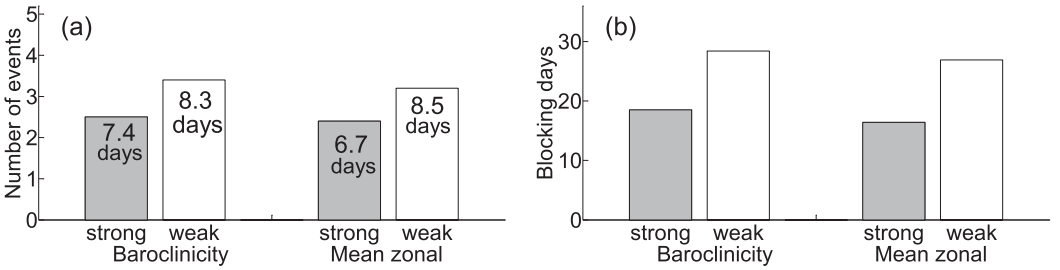

FIG. 5. Frequencies of yearly mean UB (a) events and (b) days for the strong (gray) and weak (white) MWW and VS winters during 1951–2015. The number in each box in (a) denotes the mean blocking duration.

weak MWW or VS. A strong (weak) MWW or VS winter is identified if the normalized U_{300} or VS (over the UB region) is $\geq +1.0$ (≤ -1.0) standard deviations (STDs). Because a strong VS of the MWW corresponds, for the most part, to a strong MWW in the upper troposphere as revealed above, the strong (weak) MWW and VS may be called a quasi-baroclinic (quasi barotropic) state. We used the 1951–2015 data to composite the strong and weak winters in order to increase the sample size.

We found 12 weak (9 strong) MWW winters and 12 weak (8 strong) VS winters during 1951–2015. Using the TM index, we found 38 (22) cases of UB events for the 12 weak (9 strong) MWW winters and 41 (20) cases of UB events for the 12 weak (8 strong) VS winters. Of these cases, 33 cases are overlapped for the weak MWW and VS winters, while 17 cases are overlapped for strong MWW and VS winters. The number of events, duration, and occurrence days per winter of the UB events are shown in Fig. 5 for the weak and strong MWW or VS winters.

We note that for the weak (strong) VS winters, the mean number of UB events is 3.4 (2.5) per winter and their mean duration is 8.3 (7.4) days, while the mean number of days with UB (occurrence days) is 28.4 (18.5) days per winter. Thus, the mean event number, mean duration, and occurrence days of UB events increase, respectively, by 36%, 12%, and 54% from a strong to weak VS winter. We performed a Monte Carlo test (Lund 1970) to quantify the statistical significance for these differences. It is found that the changes in the mean event number and occurrence days are statistically significant at the 95% confidence level, while their mean duration difference does not achieve significance at the 90% confidence level. As shown below, VS tends to mainly affect the amplitude of blocking dipole rather than its duration.

For weak (strong) MWW winters, the mean UB number is 3.2 (2.4) per winter, and the mean duration and occurrence days are 8.5 (6.7) days and 26.9 (16.4) days per winter, respectively. In this case, the mean event number, mean duration, and occurrence days of UB events increase, respectively, by 33%, 27%, and 64% as the MWW changes from a strong to a weak state. The difference of the mean duration is statistically significant only at the $p < 0.10$ level, while the differences in the mean event number and occurrence days are statistically significant at $p < 0.05$. Thus, both the weak VS and MWW as a quasi-barotropic condition are favorable for increased frequency (days) and persistence (long duration) of UB events. In particular, the mean duration and occurrence days of the UB events appear to be more sensitive to mid–high-latitude mean westerly winds than to VS, although the occurrence days of the UB pattern are also significantly influenced by the strength of VS. These results are not reported in previous studies (e.g., Luo et al. 2016a).

b. *What determines time-mean UB and temperature anomalies?*

To identify the influences on the intensity, position, and shape of the time-mean UB patterns, we show the time-mean 500-hPa Z and SAT anomalies averaged from lag -2 to lag $+2$ days when the UB is relatively strong, where lag 0 denotes the day when the UB peaks (as defined in Luo et al. 2016a) in Fig. 6 for strong and weak MWW winters. Similar results are obtained for a time mean from lag -5 to 5 days or from the start to the end of the blocking event (not shown). The UB anticyclonic anomaly is much stronger and farther to the west for a strong (Fig. 6a) than for a weak (Fig. 6b) MWW winter. The same is true for the VS variation (not shown). We further see that for weak MWW winters (Fig. 6b) the cold anomalies cover a widespread area that spans the Middle East, southeastern Europe, and central and East Asia. However, for strong MWW winters (Fig. 6a) the cold anomalies are located on the upstream side of the Ural region and have a narrower area that spans central and southern Europe and the Middle East, although the blocking anticyclone is strong. Figure 6c (Fig. 6d) shows the 850-hPa Z anomaly and its corresponding horizontal wind vectors averaged from lag -2 to 2 days for strong (weak) MMW winters. It is obvious that the UB has a barotropic structure because its anticyclonic circulation is also strong in the lower troposphere near the same

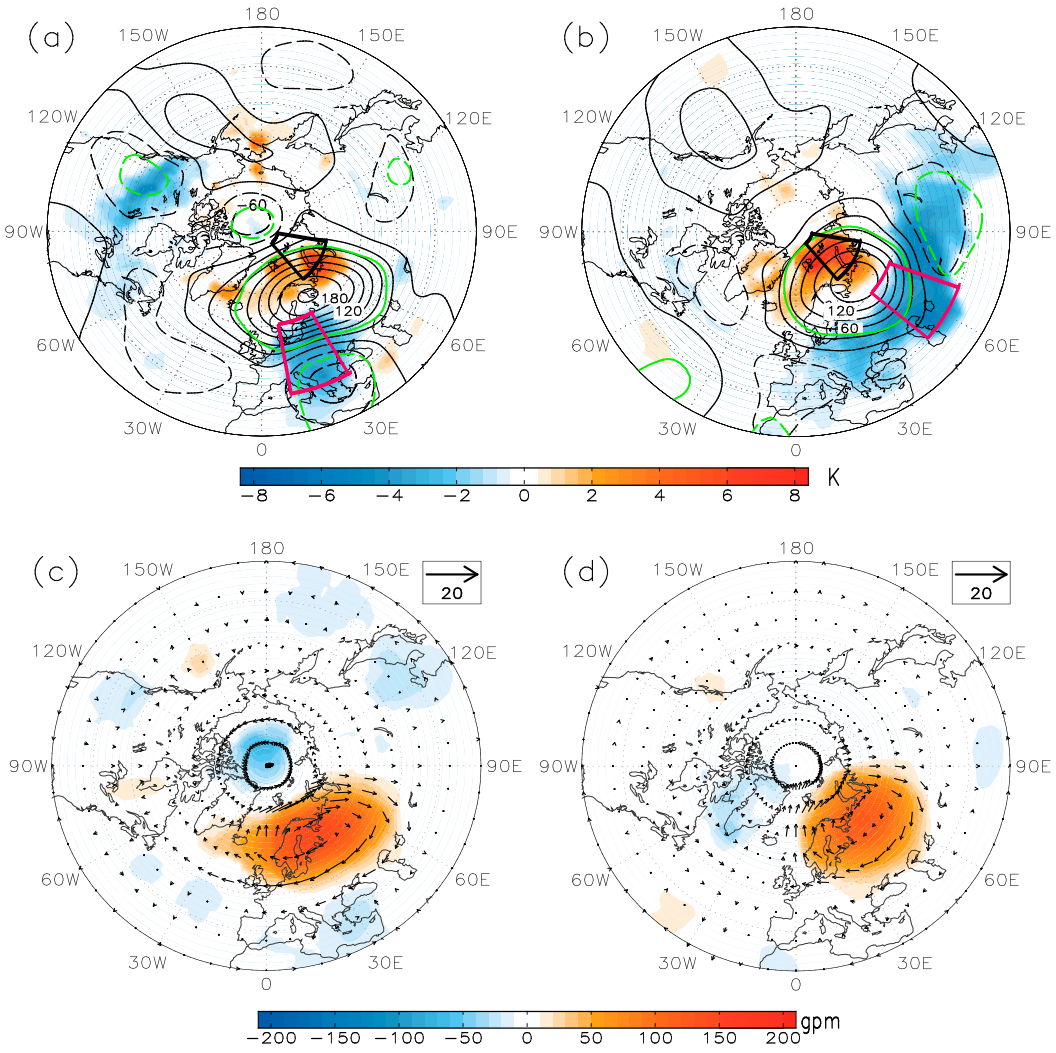

FIG. 6. (a),(b) Time-mean 500-hPa geopotential height (contours; gpm) and SAT (color shading; °C) anomalies and (c),(d) time-mean 850-hPa geopotential height anomaly (color shading; gpm) and its horizontal wind vector (arrows; m s^{-1}) only plotted for the 95% confidence level area (plotted from the north of 30°N), averaged from lag −2 to lag +2 days during the life cycle of UB events (lag 0 denotes the UB peak) for (a),(c) strong (22 cases) and (b),(d) weak (38 cases) MWW winters. The black trapezoid denotes the BKS region, while the red one represents southeastern Europe in (a) and central Asia in (b). In (a) and (b), the green contour contains the region that is above the 95% confidence level.

location (Figs. 6c,d). This shows that the Siberian high is strong (Figs. 6c,d) when the UB is strong (Figs. 6a,b), although it is clear that these two have different characteristics in that the Siberian high, in contrast to Ural blocking, is a semipermanent shallow system confined in the lower troposphere (Honda et al. 2009; Inoue et al. 2012). A detailed examination of the links between Ural blocking and the Siberian high is beyond the scope of the present study. The above composite results are also similar for the detrending of the height and temperature fields (not shown).

To understand the role of the UB pattern in producing temperature anomalies over Eurasia, one can diagnose the contributions of different processes to the SAT changes. The UB-related change of the SAT includes four parts: $\partial_t T_{\mathrm{IR}}$, $\partial_t T_{\mathrm{SLH}}$, $\partial_t T_{\mathrm{advection}}$, and $\partial_t T_{\mathrm{adiabatic}}$, which denote the SAT anomaly due to changes in, respectively, surface downward infrared radiation (IR), sensible and latent heat (SLH) fluxes, horizontal temperature advection, and adiabatic warming–cooling induced by vertical motions. We approximate these terms as $\partial_t T_{\mathrm{advection}} = -\overline{\mathbf{v}} \cdot \nabla T' - \mathbf{v}' \cdot \nabla \overline{T} - \mathbf{v}' \cdot \nabla T'$ and $\partial_t T_{\mathrm{adiabatic}} = S_P \omega$ at 850 hPa (Lee et al. 2011), where $\overline{\mathbf{v}}$ and $\overline{T}$ are the monthly mean horizontal wind vector and temperature fields, $\mathbf{v}'$ and T' are low-frequency

(7–31 days) horizontal wind vector and temperature anomalies, respectively, $S_P = -(T/\theta)(\partial\theta/\partial p)$ is the static stability, θ is the potential temperature, $\omega = dp/dt$, and p is the pressure. The calculation shows that $\partial_t T_{\text{adiabatic}}$ over Eurasia is a small term compared to other terms except over the Tibetan Plateau. Thus, the result for $\partial_t T_{\text{adiabatic}}$ is not shown below.

Figure 7 shows the maps of the anomalies in downward IR, SLH fluxes, and horizontal temperature advection [its unit is changed from $\mathrm{K\,s^{-1}}$ to $\mathrm{W\,m^{-2}}$ following the approach of Alexeev et al. (2005)] averaged from lag −2 to 2 days of the UB. It is seen that there are large positive anomalies over the BKS and its adjacent region in all four of these heat flux components (red areas in Fig. 7), giving rise to positive BKS SAT anomalies. This implies that all these processes (especially SLH fluxes) contribute to the surface warming over the BKS. Negative downward IR radiation anomalies are mainly confined in a narrow region across southern Europe and parts of central Asia for strong MWW winters (Fig. 7a), while they are more intense and extend to central and East Asia and parts of southern Europe for weak MWW winters (Fig. 7d). It is also seen that the negative SLH fluxes (Figs. 7b,e) are relatively weak over midlatitude Eurasia and are more confined to eastern Europe compared to the IR radiation, and they are comparable for the weak and strong MWW winters (this is also true for the temperature advection; Figs. 7c,f). The clear difference in the IR could help maintain the large SAT difference between the weak and strong MWW winters (Figs. 6a,b). We realize that the downward IR is controlled by lower-tropospheric temperature and water vapor content (Zhang et al. 1995; Park et al. 2015), which in turn are coupled with the SAT. Thus, the SAT and IR radiation anomalies are physically coupled together and should be consistent with each other. Nevertheless, the negative IR anomalies are the primary factor that helps maintain the widespread cold SAT anomalies over Eurasia during weak MWW winters (Fig. 6b).

We now investigate what characteristics of the UB produce the different IR fluxes (Figs. 7a,d) and cold anomalies over Eurasia (Figs. 6a,b) during the weak and strong MWW winters and do this by following the daily evolution of the UB patterns for the two types of winters. Figure 8a shows that for strong MWW winters a weak anticyclonic anomaly appears downstream of the Ural Mountains at lag −10 days. Its intensification is slow from lag −10 to −6 days, and it undergoes a slow retrogression (i.e., westward motion). The retrogression then speeds up as its amplitude peaks at lag 0 day, when it is on the west side of the Ural region. Subsequently this blocking anticyclone retrogrades rapidly and enters the North Atlantic at lag +2 day. From lag +2 to +8 days, it moves to Greenland and stays there and maintains its rather strong intensity until lag +8 day. The rapid retrogression of the UB anticyclone results in little time spent over the Ural region. The areas of the cold SAT anomalies change with the retrograding blocking anticyclone, and they are seen mainly over Europe during the period from lag −2 to +6 days. It needs to be pointed out that all the composite results are based on the removal of the trends in the MWW and VS time series.

The synoptic evolution is very different for weak MWW winters (Fig. 8b), during which we see that a weak UB anticyclone appears over the BKS region near the Ural region at lag −10 day. It slowly intensifies and shifts southeastward from lag −10 to −4 days. It then grows into a typical UB pattern and moves slightly westward from lag −4 to 0 days. This UB pattern has a weak westward displacement from lag 0 to 4 days. It hardly moves once over the Ural region. Such a quasi-stationary blocking pattern can lead to persistent cooling (warming) over its southeast (north) side owing to the UB-related cooling (warming) associated with the negative (positive) downward IR, anomalous horizontal temperature advection, SLH fluxes, and adiabatic cooling (warming) (not shown). For this case, the cold and warm anomalies (color in Fig. 8b) are more intense and widespread than those for strong MWW winters (Fig. 8a). Similar results were also found for UB events for strong and weak VS winters (not shown). On the other hand, the SAT anomaly over the BKS region becomes negative after the UB migrates into the North Atlantic near Greenland during the period from lag +4 to 8 days during strong MWW winters (Fig. 8a). This indicates that the rapidly retrograding UB can act as a positive (negative) feedback on the Arctic warming over the BKS region during its growing (decaying) phase. This result is different from that of a quasi-stationary UB for weak MWW winters, always have a positive feedback on the BKS warming during its life cycle (Fig. 8b).

While Screen and Simmonds (2014) noted that amplified planetary waves are important for extreme weather events, our results below further reveal that the quasi stationarity and persistence of specific UB patterns are especially important for the magnitude and location of the cold events. In contrast, the amplitude of blocking (planetary waves) is not important if it moves rapidly westward. Below we examine how the movement, persistence, and amplitude of UB patterns may affect cold and warm extremes.

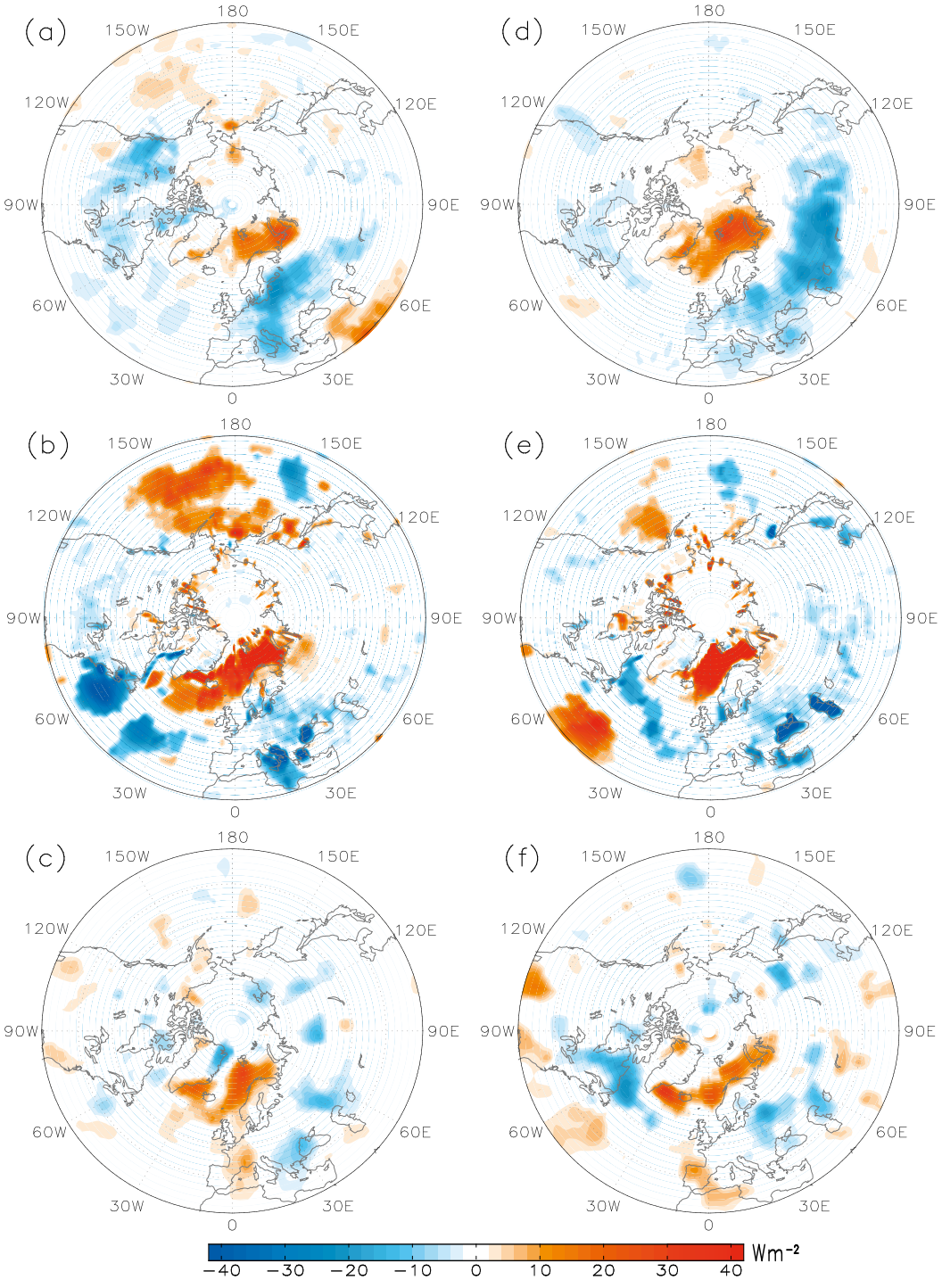

FIG. 7. Time-mean anomalies (W m^{-2}) of (a) surface downward IR radiation, (b) the sum of surface sensible and latent heat flux, and (c) 850-hPa horizontal temperature advection averaged from lag −2 to 2 days for the strong MWW winters. (d)–(f) As in (a)–(c), but for the weak MWW winters. The color shading areas that are above 95% confidence level are plotted.

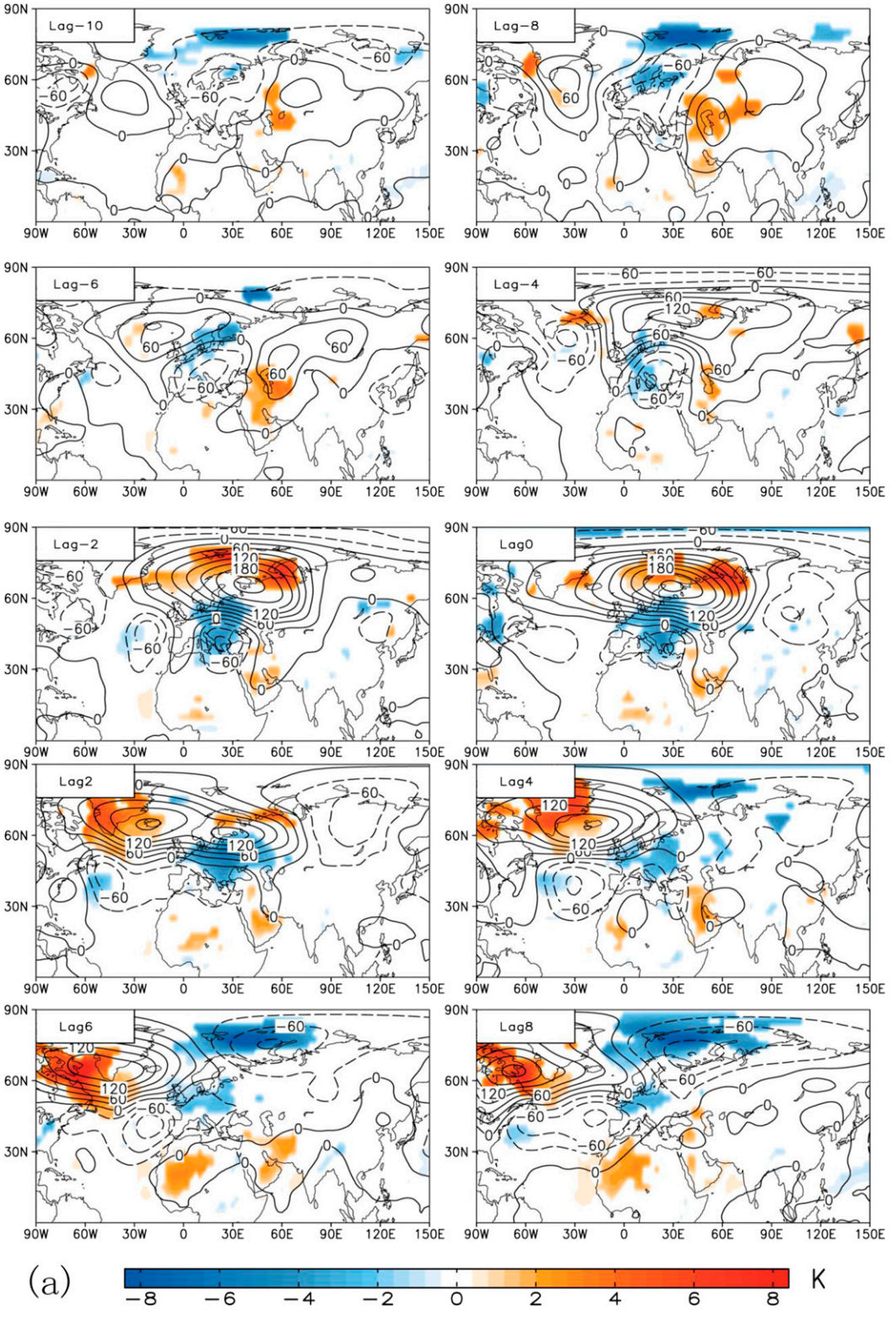

FIG. 8. Composite daily 2-day-interval 500-hPa geopotential height (contours; gpm) and SAT (color shading; K) anomalies during the life cycle of the UB events—from lag −10 to lag 8 days for (a) strong and (b) weak MWW winters during 1951–2015 based on NCEP–NCAR reanalysis data. The color shading areas that are above 95% confidence level are plotted.

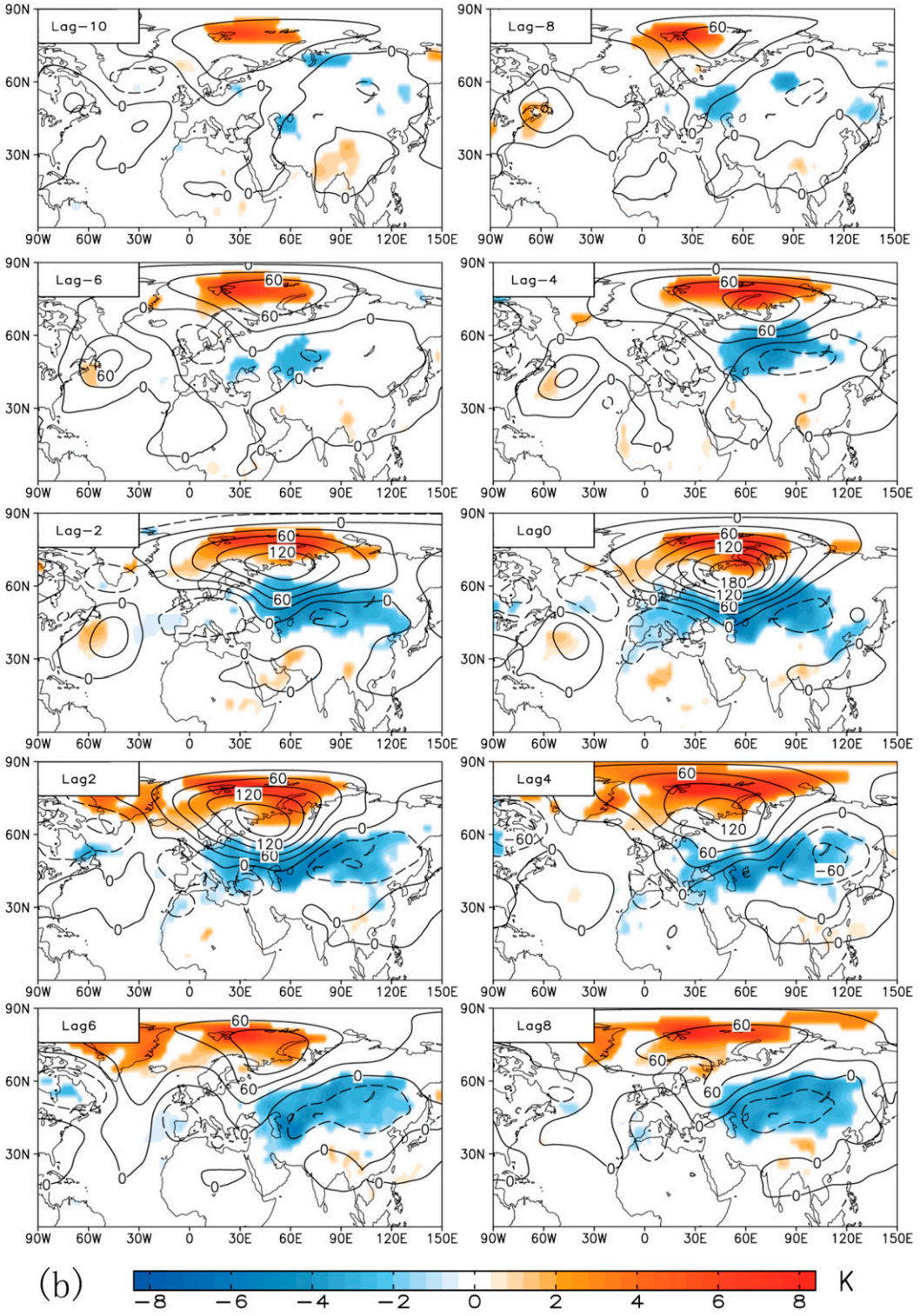

FIG. 8. (*Continued*)

5. Cold and warm extremes over Eurasia and their link to the movement, persistence, and amplitude of UB patterns

Although the strengths of MWW and VS can affect the regional extent, intensity, and persistence of cold and warm anomalies through modulating the persistence, movement, and strength of the UB pattern as revealed above, it is necessary to quantify the relationship between the UB pattern and cold and warm SAT extremes. We first define the area-averaged daily 500-hPa height anomaly over the region 60°–70°N, 30°–60°E as the daily intensity or amplitude of the UB pattern by considering its westward movement for weak and strong MWW cases, although the chosen area is located in the west of the mean position of UB events (Diao et al. 2006). Furthermore, the daily SAT anomaly averaged over the region 60°–85°N, 40°–80°E is defined as the daily UB-related warm temperature anomaly ΔT_H in high-latitude Eurasia because it is wide and covers the BKS region. On the other hand, because the strong cold anomalies appear over Europe (40°–60°N, 10°–30°E; red box in Fig. 6a) and central Asia (40°–60°N, 50°–70°E; red box in Fig. 6b) for strong and weak MWW winters, respectively, we define the daily SAT anomalies ΔT_E and ΔT_{CA} averaged over the two regions as the measures of daily UB-associated cold temperature anomalies over Europe and central Asia. The same definitions may be made for strong and weak VS winters because they have SAT anomaly patterns similar to those for strong and weak MWW winters (not shown).

a. *Cold and warm anomalies and their relationships with UB patterns*

As seen from the composite daily UB strengths in Fig. 9a for strong and weak MWW winters, the UB is more persistent over the Ural region for the weak (dashed line in Fig. 9a) than strong MWW winters (solid line in Fig. 9a), while it is more intense during strong MWW winters (solid line in Fig. 9a). This implies that the large (small) amplitude UB pattern has a short (long) lifetime over the Ural region. Comparisons between Fig. 9a and Fig. 9b suggest that the long-lasting warming in high-latitude Eurasia (including the BKS) is associated with more persistent UB patterns during weak MWW winters. Further, Figs. 9c,d reveal that the magnitude and persistence of cold anomalies over Europe (central Asia) depend strongly on the amplitude of the UB pattern linked to the different strength of the MWW. The UB-related cold anomaly over Europe (Fig. 9c) is more intense for a strong (solid line in Fig. 9c) than for a weak MWW (dashed line in Fig. 9c), while the high-latitude warming is relatively weak for a strong MWW (solid line in Fig. 9b). This reflects that the large-amplitude UB pattern has a large effect on cold anomalies over Europe, rather than over central or East Asia, because it shows a marked retrogression. While the UB has small amplitude for a weak MWW winter, the UB-related cold anomalies over central Asia are much more intense and persistent than is a strong MWW winter (solid line in Fig. 9d) because they can correspond to a persistent cooling over central Asia owing to their strong quasi stationarity and long persistence in the Ural region (Fig. 9b). Thus, it appears that the quasi-stationary and persistent UB pattern being small amplitude, which is often associated with the weak MWW, has a prominent effect on cold anomalies over central and East Asia. This indicates that the cooling over central Asia is closely related to the quasi stationarity and persistence of UB rather than its amplitude under a weak MWW condition. This result is also held for weak VS (not shown). The above results are different from previous findings of Francis and Vavrus (2012), Screen and Simmonds (2014), and Walsh (2014), who emphasized the role of the large amplitude of amplified planetary waves in the midlatitude weather.

We show the area-averaged DJF-mean SAT anomalies over the BKS $\Delta\overline{T}_{\mathrm{BKS}}$, Europe $\Delta\overline{T}_E$, and central Asia $\Delta\overline{T}_{\mathrm{CA}}$ in Fig. 10 for nondetrended (Fig. 10a) and detrended (Fig. 10b) cases. As to the winter-mean SAT anomaly, we find that $\Delta\overline{T}_E$ over Europe (solid line in Fig. 10) and $\Delta\overline{T}_{\mathrm{CA}}$ over central Asia (dashed line in Fig. 10) exhibit negative correlations of -0.55 and -0.37 (-0.55 and -0.35) with the UB days for a nondetrended (detrended) case in Fig. 10a (Fig. 10b). The negative correlations of the detrended $\Delta\overline{T}_E$ and $\Delta\overline{T}_{\mathrm{CA}}$ time series with the UB mean duration (dashed line in Fig. 3c), which are -0.27 and -0.39, respectively, are also statistically significant at the 95% confidence level, while the detrended $\Delta\overline{T}_{\mathrm{BKS}}$ over the BKS has a positive correlation of 0.27 ($p = 0.05$) with the UB days. As noted in Luo et al. (2016a, their Fig. 8a) the presence of the blocking pattern can induce a quasi-biweekly dipole temperature anomaly with high-latitude warming and midlatitude cooling. Thus, it is inevitable that there are high correlations of $\Delta\overline{T}_E$, $\Delta\overline{T}_{\mathrm{CA}}$, and $\Delta\overline{T}_{\mathrm{BKS}}$ with the UB days or mean duration. The high-latitude warming and midlatitude cooling can also be explained by the meridional mass circulation (Yu et al. 2015a,b), which suggests that warm air masses are transported into the Arctic in upper levels and cold air masses in lower levels are transported out of the Arctic into midlatitudes. Moreover, a comparison with Fig. 3b shows that the variations of the detrended $\Delta\overline{T}_{\mathrm{CA}}$ and $\Delta\overline{T}_{\mathrm{BKS}}$ seen in Fig. 10b can explain changes in the MWW and VS (Fig. 3b).

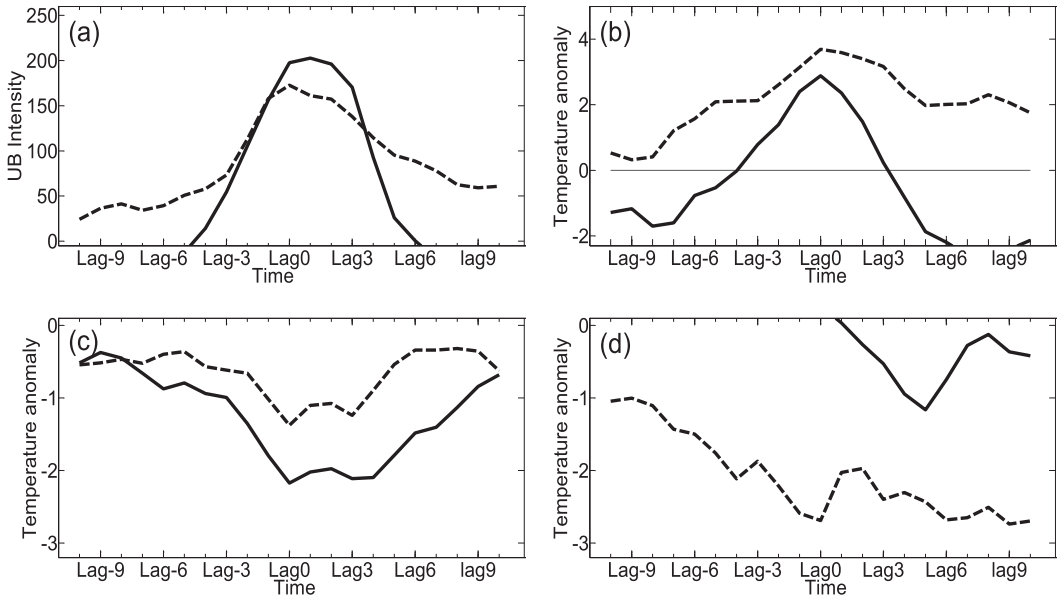

FIG. 9. Composite daily time series (a) 500-hPa geopotential height anomaly (gpm) averaged over 60°–70°N, 30°–60°E; (b) SAT anomalies (ΔT_H; K) averaged over the BKS region (60°–85°N, 40°–80°E); (c) SAT anomalies (ΔT_E; K) averaged over Europe (40°–60°N, 10°–30°E); and (d) SAT anomalies (ΔT_{CA}; K) averaged over central Asia (40°–60°N, 50°–70°E) during the UB life cycle for strong (solid) and weak (dashed) MWW winters.

On the other hand, it is also seen from Fig. 10a that while the SAT anomaly over central Asia has an increased trend during 1970–99, it has a lower value during 2000–15 (blue line in Fig. 10a). This period corresponds to a Northern Hemisphere (NH) winter warming hiatus epoch taking place over central Asia during 2000–15 (Dai et al. 2015). But this phenomenon is not apparent over Europe (green line in Fig. 10a). Because the decrease of the SAT anomaly over central Asia (blue line in Fig. 10a) corresponds to an increased UB frequency (days) (solid line in Fig. 3c), it is inferred that the NH winter warming hiatus observed in the recent decade (2000–15) is linked with the abrupt decline of the BKS sea ice or enhanced BKS warming during 2000–15 through increasing the quasi stationarity and persistence of UB events. This problem will be further investigated in another paper.

To quantify the contributions of blocking days to cold and warm anomalies we present the probability density functions (PDFs) of daily SAT anomalies $\Delta\overline{T}_E$, $\Delta\overline{T}_{\mathrm{CA}}$, and $\Delta\overline{T}_{\mathrm{BKS}}$ averaged over Europe, central Asia, and BKS in Fig. 11 for the 4653 nonblocking (1213 blocking) days of all winters during 1951–2015. For the nonblocking days these PDFs show a warm shift of the mean temperature anomaly over Europe (red curve in Fig. 11a) and central Asia (red curve in Fig. 11b) but a shift to the cold side over the BKS (red curve in Fig. 11c). However, the PDFs for the blocking days (blue curve in Fig. 11) show the opposite shifts to those without UB (red curve in Fig. 11). In other words, the cold anomalies over Europe and central Asia and a warm anomaly over the BKS can appear with the UB events. A similar result is found for 1979–2015 (not shown).

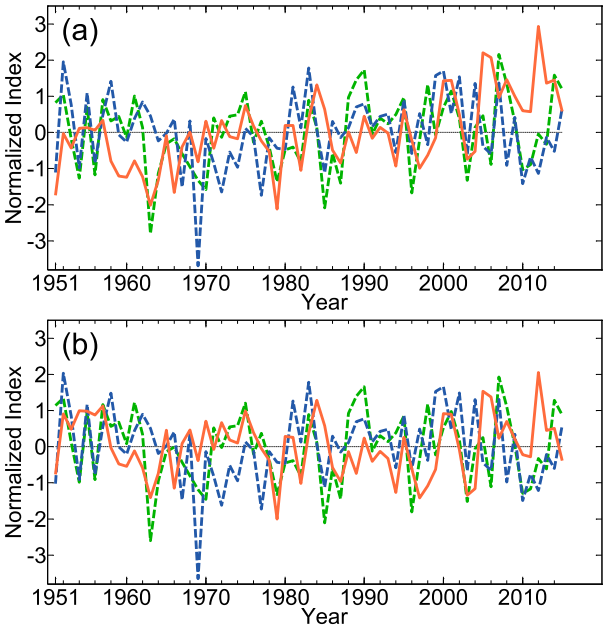

FIG. 10. Time series of normalized winter-mean SAT anomaly averaged over Europe $\Delta\overline{T}_E$ (40°–60°N, 10°–30°E; green), central Asia $\Delta\overline{T}_{\mathrm{CA}}$ (40°–60°N, 50°–70°E; blue), and BKS $\Delta\overline{T}_{\mathrm{BKS}}$ (70°–85°N, 40°–80°E; red) during 1951–2015 for (a) nondetrended and (b) detrended cases.

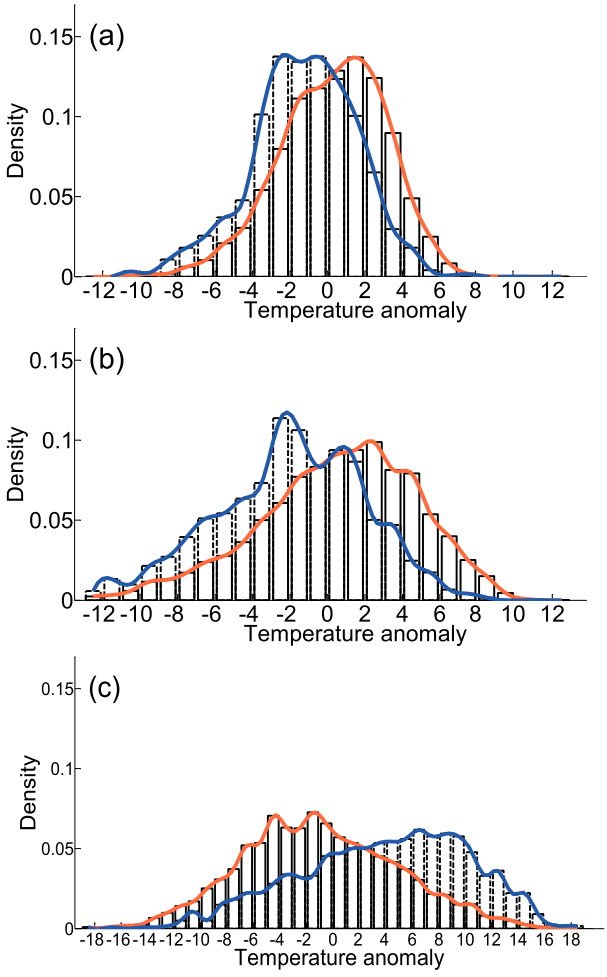

FIG. 11. Probability density distributions of daily SAT anomalies averaged over (a) Europe, (b) central Asia, and (c) BKS for 4653 nonblocking days (red curve) and 1213 blocking days (blue curve) of all winters during 1951–2015. In each panel, the red or blue line denotes a no-parameter fitting of the probability distribution. The shift between the peaks of the two samples (red and blue curves) is statistically significant at the 99% confidence level in a Monte Carlo test.

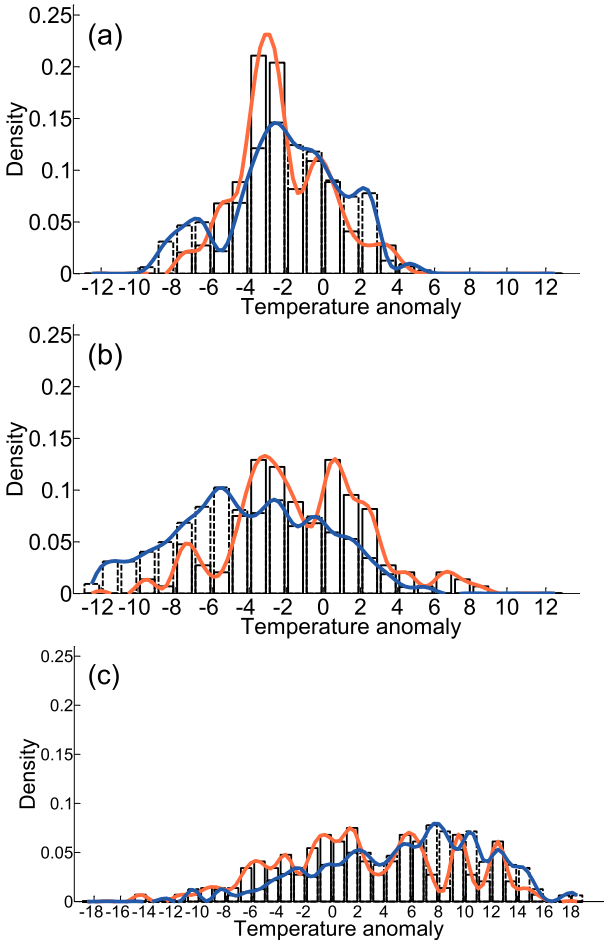

FIG. 12. As in Fig. 11, but for 147 UB days of strong MWW winters (red) and 322 UB days of weak MWW winters (blue) during 1951–2015.

We also show the PDFs of daily SAT anomalies associated with UB days over Europe, central Asia, and BKS in Figs. 12a–c for strong (red) and weak (blue) MWW winters. For the strong case the PDFs of the UB-associated daily SAT anomalies show a shift of the mean temperature anomaly value to the colder side over Europe (red in Fig. 12a) than for a weak case (blue in Fig. 12a). This reflects that the strong MWW can more significantly affect cold anomalies over Europe than the weak MWW. In contrast, for a weak MWW, the PDF of the UB-associated daily SAT anomalies shows a stronger shift toward the colder side over central Asia (blue in Fig. 12b) than for a strong MWW (red in Fig. 12b). Thus, it suggests that under the weak MWW conditions the UB pattern can significantly affect cold anomalies over central Asia and its adjacent region, rather than mainly over Europe. It is also found that the PDF of the UB-associated daily SAT anomalies over the BKS shifts to the warmer side (blue in Fig. 12c) for a weak MWW than for a strong MWW, thus indicating that the UB pattern could lead to a more marked warming over the BKS for a weak MWW than for a strong MMW. Similar results are also found for the weak (strong) VS case (not shown).

b. *The persistence of cold and warm extremes and its link with the background conditions*

Here, we define a warm (cold) extreme event in terms of the area-averaged daily SAT anomaly +5°C (−5°C) from the mean that persists for at least three consecutive days at a given location (following the procedure of Dole et al. 2011). Similar results are found for other threshold specifications (not shown). We show the event

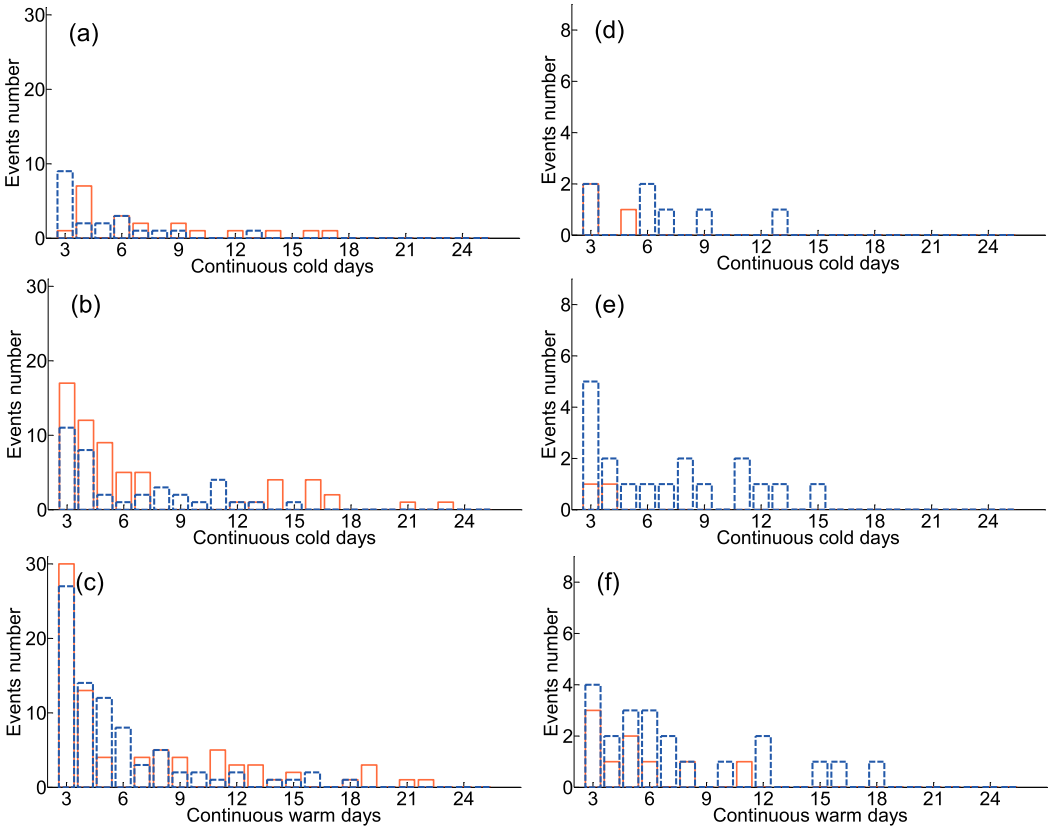

FIG. 13. The event number against the continuous days of cold extremes over (a),(d) Europe and (b),(e) central Asia, and warm extremes over (c),(f) BKS with threshold of ±5°C for the (a)–(c) 4653 nonblocking (red) and 1213 UB days (blue) of all winters and for the (d)–(f) UB days of strong (red) and weak (blue) MWW winters during 1951–2015.

numbers against the continuous days of cold extremes over Europe and central Asia and warm extremes over the BKS in Figs. 13a–c for the 4653 nonblocking and 1213 blocking days of all winters during 1951–2015. The results are shown in Figs. 13d–f for strong and weak MWW winters. A comparison between Figs. 13a–c and Figs. 13d–f clearly shows that the persistence of cold and warm extremes over Eurasia depends on the strength of the MWW.

The cold extremes over Europe are seen to be both less frequent and less persistent than over central Asia even under the weak MWW condition (Fig. 13d). The UB has a dominant contribution to cold extremes persisting from 4 to 15 days over central Asia for a weak MWW (Fig. 13e). We also see that a large part of warm extremes over the BKS are related to UB events under the weak MWW condition (Fig. 13f). Similar results are found for the weak or strong VS condition (not shown). Thus, we conclude that the UB-related warm extremes over the BKS and cold extremes over Eurasia are favored by quasi-stationary UB events under weak MWW or VS conditions.

Our statistical analysis further reveals that 50% (40%) of the winters with strong BKS warming (DJF-mean $\Delta\overline{T}_{\mathrm{BKS}} \geq 1.0$ STDs) correspond to weak VS (MWW) winters over Eurasia during 1951–2015. This is easily explained because the strong background BKS warming weakens the north–south temperature gradient and then reduces the mean westerly wind and its vertical shear. However, if the criterion is reduced to 0.5 STDs, 47% (53%) of the winters with DJF-mean $\Delta\overline{T}_{\mathrm{BKS}} > 0.5$ STDs correspond to weak VS (MWW) winters. Thus, the magnitude of the percentage of warm BKS winters corresponding to weak VS or MWW shows that the background conditions not only depend on the Arctic warming associated with the sea ice loss over the BKS but might also depend on other factors like the PDO (Screen and Francis 2016), troposphere–stratosphere coupling, and European cooling trend (Cohen et al. 2014). Thus, the BKS warming-associated UB patterns may have different features (duration, position, and strength) if the background conditions for VS or MWW over Eurasia are different. For example, under strong VS/MWW conditions the blocking moves westward rapidly and it is rather strong (Fig. 8a).

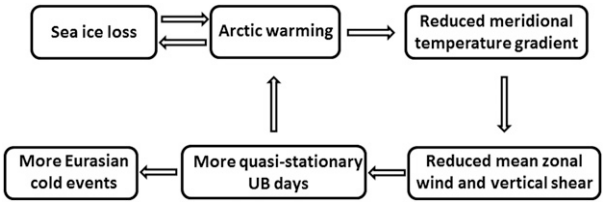

FIG. 14. A schematic diagram used to describe the impact of Arctic sea ice loss over the BKS on UB and the feedback of the UB on the Arctic warming.

Such cold extremes over Europe and warm extremes over the BKS associated with such strong blocking are less persistent and distinct. Thus, the magnitude and occurrence region of the UB-associated cold anomalies over Eurasia and warming over the BKS are dependent not only on the BKS warming prior to the UB onset but also on the background conditions of VS and MWW over mid–high-latitude Eurasia, with the latter being modified by the BKS warming itself.

6. Conclusions and discussion

We have examined the relationships among the winter Arctic warming and sea ice loss over the Barents and Kara Seas (BKS), the mean westerly wind (MWW) and its vertical shear (VS), the Ural blocking (UB), and winter cold events in midlatitude Eurasia. Regression analyses undertaken with NCEP–NCAR reanalysis and ERA-Interim data show that the Arctic sea ice loss corresponds to a strong anticyclonic anomaly over the Ural blocking region and its north side, possibly through the effect of the BKS warming associated with the sea ice loss. The DJF-mean meridional temperature gradient (MTG) over Eurasia exhibits a strong negative correlation with the BKS warming, while the MWW and VS over Eurasia have a significant positive correlation with the MTG strength, which can be explained using the thermal wind equation. The MWW and VS exhibit an enhanced negative correlation with the intensified background BKS warming during P2. Thus, the weaker MWW and VS tend to occur during P2 because the background BKS warming is more intense during P2 than during P1 (Fig. 1b). It is also found that the blocking days and mean duration of UB events exhibit significant negative correlations with the MWW and VS strength that was relatively strong (weak) during 1979–99 (2000–15). Winter UB days increase by 64% (54%) from 16.4 (18.5) to 26.9 (28.4) days per winter from the strong to weak MWW (VS) winters during 1951–2015.

Further analyses show that when the MWW or VS is strong, as frequently observed during 1979–99, the UB pattern is both strong and rapidly westward moving. In this case, cold events occur mainly over Europe and are less persistent, and the UB-induced high-latitude warming (as a positive feedback of the UB patterns on the BKS warming) is also weak and less persistent. However, when the MWW or VS is weak, as frequently observed during 2000–15 (Figs. 2 and 3), the UB anticyclone is relatively weak, moves slowly westward, and becomes persistent (dashed line in Fig. 9a) and quasi stationary. In this case, large cold anomalies are found to be strong (Fig. 12) and long lived over a widespread region that spans central and East Asia (dashed line in Fig. 9d). Moreover, the UB-related high-latitude warming over the BKS is also stronger and more persistent, so that its positive feedback on the BKS warming is strong. The widespread cold anomalies over Eurasia are maintained primarily by negative downward IR associated with the UB in weak MWW winters. Therefore, we conclude that under the weak MWW or VS condition, which is the case for 2000–15, the impacts of the UB patterns on both Eurasian cold events and Arctic warming (and thus sea ice loss) over the BKS are more pronounced because of the increased quasi stationarity and persistence of the UB events. Thus, the large warming since 2000 over the BKS weakens the MTG, MWW, and VS, which increases the quasi stationarity and persistence of UB events, which in turn lead to more widespread cold events over Eurasia (Fig. 12) and further enhance the warming over the BKS, as illustrated in Fig. 14. Because the cooling over central Asia occurs mainly during 2000–15 (blue line in Fig. 10) and is related to the quasi-stationary and persistent UB, the NH winter warming hiatus observed in the recent decade (2000–15) is likely associated with the quasi-stationary and persistent UB linked to the background Arctic warming or sea ice loss over the BKS. It seems that the recent winter warming hiatus occurs together with the recent rapid decline of Arctic sea ice because they began from 2000. In particular, cold (warm) extremes are more persistent over central Asia (BKS) for weak than for strong MWW or VS winters (Figs. 13d–f).

As revealed above, the large-amplitude UB pattern is not important for strong extreme cold events and Arctic warming because it moves westward rapidly. Instead, the quasi stationarity and persistence of the UB pattern, rather than its amplitude, are crucial for the intensity, persistence, and occurrence region of the winter cold anomalies over Eurasia and the BKS warming. This result is different from previous findings (Francis and Vavrus 2012; Liu et al. 2012; Screen and Simmonds 2013a,b; Cohen et al. 2014; Walsh 2014), which emphasized the role of high-amplitude waves (such as blocking). While our study reveals that the severity and occurrence region of cold events over Eurasia depend strongly on the quasi stationarity and persistence of the UB events, it is still unclear how the UB activity is

linked to changes in the background conditions of MWW and VS over Eurasia, although the phase of the NAO can affect the UB and European blocking (Luo et al. 2007; Yao and Luo 2014; Luo et al. 2016b). In particular, why the UB becomes quasi stationary and long lived under the weak MWW or VS condition is not theoretically clarified. This is investigated in Part II.

Acknowledgments. The first two authors acknowledge the support from the National Key Research And Development Program of China (2016YFA0601802) and the National Natural Science Foundation of China (Grants 41505075, 41430533, and 41375067). A. Dai is supported by the U.S. National Science Foundation (Grant AGS-1353740), the U.S. Department of Energy's Office of Science (Award DE-SC0012602), and the U.S. National Oceanic and Atmospheric Administration (Award NA15OAR4310086). I. Simmonds was supported by Australian Research Council Grant DP 160101997. The authors thank three anonymous reviewers for their useful suggestions in improving this paper.

APPENDIX

Thermal Wind Equation and Its Physical Meaning

The zonal component of the thermal wind equation (in pressure coordinates) can be written as

$$\frac{\partial u_g}{\partial \ln p} = \frac{R}{f}\frac{\partial \overline{T}}{\partial y}, \tag{A1}$$

where u_g is the zonal component of geostrophic wind, p is the pressure, y is the meridional coordinate, $\overline{T}$ is the mean air temperature, R is the gas constant, and f is the Coriolis parameter.

Integrating from p_2 to p_1 we get

$$u_g(p_1) - u_g(p_2) = \frac{R}{f}\int_{\ln p_2}^{\ln p_1} \frac{\partial \overline{T}}{\partial y} d\ln p. \tag{A2}$$

Here, if we take $p_1 = 300\,\text{hPa} = [(200 + 400\,\text{hPa})/2]$, and $p_2 = 725\,\text{hPa} = [(600 + 850\,\text{hPa})/2]$ as the upper and lower levels of the troposphere; thus, the vertical shear of the mean zonal wind in the troposphere is

$$\Delta U = u_g(p_1) - u_g(p_2) = \frac{R}{f}\int_{\ln p_2}^{\ln p_1} \frac{\partial \overline{T}}{\partial y} d\ln p. \tag{A3}$$

Integrating Eq. (A1) from 1000 hPa to p_2 yields

$$u_g(p_2) = u_g(1000) + \frac{R}{f}\int_{\ln(1000)}^{\ln p_2} \frac{\partial \overline{T}}{\partial y} d\ln p. \tag{A4}$$

Substituting Eq. (A4) into Eq. (A3) we get

$$u_g(p_1) = u_g(1000) + \Delta U + \frac{R}{f}\int_{\ln(1000)}^{\ln p_2} \frac{\partial \overline{T}}{\partial y} d\ln p. \tag{A5}$$

It is clear that there is a linear relationship between the mean zonal wind U_{300} and ΔU (VS) according to Eq. (A5). The Arctic warming does not certainly affect VS if it takes place in the lower troposphere below 725 hPa. However, if the Arctic warming can gradually penetrate into the whole deep troposphere, it significantly changes U_{300} and ΔU through altering the meridional temperature gradients in different layers: $(R/f)\int_{\ln(1000)}^{\ln p_2}(\partial \overline{T}/\partial y)d\ln p$ and $(R/f)\int_{\ln p_2}^{\ln p_1}(\partial \overline{T}/\partial y)d\ln p$.

Equations (A4) and (A5) may be used to understand the correlation between any two of U_{300}, ΔU, and MTG as noted in section 3.

REFERENCES

Alexeev, V. A., P. L. Langen, and J. R. Bates, 2005: Polar amplification of surface warming on an aquaplanet in "ghost forcing" experiments without sea ice feedbacks. *Climate Dyn.*, **24**, 655–666, doi:10.1007/s00382-005-0018-3.

Cohen, J., and Coauthors, 2014: Recent Arctic amplification and extreme mid-latitude weather. *Nat. Geosci.*, **7**, 627–637, doi:10.1038/ngeo2234.

Dai, A., J. C. Fyfe, S.-P. Xie, and X. Dai, 2015: Decadal modulation of global-mean temperature by internal climate variability. *Nat. Climate Change*, **5**, 555–559, doi:10.1038/nclimate2605.

Diao, Y., J. Li, and D. Luo, 2006: A new blocking index and its application: Blocking action in the Northern Hemisphere. *J. Climate*, **19**, 4819–4839, doi:10.1175/JCLI3886.1.

Dole, R., and Coauthors, 2011: Was there a basis for anticipating the 2010 Russian heat wave? *Geophys. Res. Lett.*, **38**, L06702, doi:10.1029/2010GL046582.

Fang, Z., and J. M. Wallace, 1994: Arctic sea ice variability on a timescale of weeks and its relation to atmospheric forcing. *J. Climate*, **7**, 1897–1914, doi:10.1175/1520-0442(1994)007<1897:ASIVOA>2.0.CO;2.

Francis, J. A., and E. Hunter, 2007: Drivers of declining sea ice in the Arctic winter: A tale of two seas. *Geophys. Res. Lett.*, **34**, L17503, doi:10.1029/2007GL030995.

——, and S. J. Vavrus, 2012: Evidence linking Arctic amplification to extreme weather in mid-latitudes. *Geophys. Res. Lett.*, **39**, L06801, doi:10.1029/2012GL051000.

——, and ——, 2015: Evidence for a wavier jet stream in response to rapid Arctic warming. *Environ. Res. Lett.*, **10**, 014005, doi:10.1088/1748-9326/10/1/014005.

Gao, Y., and Coauthors, 2015: Arctic sea ice and Eurasian climate: A review. *Adv. Atmos. Sci.*, **32**, 92–114, doi:10.1007/s00376-014-0009-6.

Honda, M., J. Inoue, and S. Yamane, 2009: Influence of low Arctic sea-ice minima on anomalously cold Eurasian winters. *Geophys. Res. Lett.*, **36**, L08707, doi:10.1029/2008GL037079.

Inoue, J., M. E. Hori, and K. Takaya, 2012: The role of Barents Sea ice in the wintertime cyclone track and emergence of a warm-Arctic cold-Siberian anomaly. *J. Climate*, **25**, 2561–2568, doi:10.1175/JCLI-D-11-00449.1.

Kug, J. S., J. Jeong, Y. S. Jang, B. M. Kim, C. K. Folland, S. K. Min, and S. W. Son, 2015: Two distinct influences of Arctic warming on cold winters over North America and East Asia. *Nat. Geosci.*, **8**, 759–762, doi:10.1038/ngeo2517.

Lee, S., T. Gong, N. C. Johnson, S. B. Feldstein, and D. Pollard, 2011: On the possible link between tropical convection and the Northern Hemisphere Arctic surface air temperature change between 1958 and 2001. *J. Climate*, **24**, 4350–4367, doi:10.1175/2011JCLI4003.1.

Liu, J., J. A. Curry, H. Wang, M. Song, and R. M. Horton, 2012: Impact of declining Arctic sea ice on winter snowfall. *Proc. Natl. Acad. Sci. USA*, **109**, 4074–4079, doi:10.1073/pnas.1114910109.

Lund, I. A., 1970: A Monte Carlo method for testing the statistical significance of a regression equation. *J. Appl. Meteor.*, **9**, 330–332, doi:10.1175/1520-0450(1970)009<0330:AMCMFT>2.0.CO;2.

Luo, D., 2000: Planetary-scale baroclinic envelope Rossby solitons in a two-layer model and their interaction with synoptic-scale eddies. *Dyn. Atmos. Oceans*, **32**, 27–74, doi:10.1016/S0377-0265(99)00018-4.

——, A. R. Lupo, and H. Wan, 2007: Dynamics of eddy-driven low-frequency dipole modes. Part I: A simple model of North Atlantic Oscillations. *J. Atmos. Sci.*, **64**, 3–28, doi:10.1175/JAS3818.1.

——, Y. Xiao, Y. Yao, A. Dai, I. Simmonds, and C. L. E. Franzke, 2016a: Impact of Ural blocking on winter warm Arctic–cold Eurasian anomalies. Part I: Blocking-induced amplification. *J. Climate*, **29**, 3925–3947, doi:10.1175/JCLI-D-15-0611.1.

——, ——, Y. Diao, A. Dai, C. L. E. Franzke, and I. Simmonds, 2016b: Impact of Ural blocking on winter warm Arctic–cold Eurasian anomalies. Part II: The link to the North Atlantic Oscillation. *J. Climate*, **29**, 3949–3971, doi:10.1175/JCLI-D-15-0612.1.

——, Y. Yao, A. Dai, I. Simmonds, and L. Zhong, 2017: Increased quasi stationarity and persistence of winter Ural blocking and Eurasian extreme cold events in response to Arctic warming. Part II: A theoretical explanation. *J. Climate*, **30**, 3569–3587, doi:10.1175/JCLI-D-16-0262.1.

Mori, M., M. Watanabe, H. Shiogama, J. Inoue, and M. Kimoto, 2014: Robust Arctic sea-ice influence on the frequent Eurasian cold winters in past decades. *Nat. Geosci.*, **7**, 869–873, doi:10.1038/ngeo2277.

Murray, R. J., and I. Simmonds, 1995: Responses of climate and cyclones to reductions in Arctic winter sea ice. *J. Geophys. Res.*, **100**, 4791–4806, doi:10.1029/94JC02206.

Newson, R. L., 1973: Response of general circulation model of the atmosphere to removal of the Arctic ice cap. *Nature*, **241**, 39–40, doi:10.1038/241039b0.

Outten, S. D., and I. Esau, 2012: A link between Arctic sea ice and recent cooling trends over Eurasia. *Climatic Change*, **110**, 1069–1075, doi:10.1007/s10584-011-0334-z.

Overland, J., K. R. Wood, and M. Wang, 2011: Warm Arctic—Cold continents: Climate impacts of the newly open Arctic Sea. *Polar Res.*, **30**, 15787, doi:10.3402/polar.v30i0.15787.

Park, D. S., S. Lee, and S. Feldstein, 2015: Attribution of the recent winter sea ice decline over the Atlantic sector of the Arctic Ocean. *J. Climate*, **28**, 4027–4033, doi:10.1175/JCLI-D-15-0042.1.

Petoukhov, V., and V. A. Semenov, 2010: A link between reduced Barents–Kara Sea ice and cold winter extremes over northern continents. *J. Geophys. Res.*, **115**, D21111, doi:10.1029/2009JD013568.

Simmonds, I., 2015: Comparing and contrasting the behaviour of Arctic and Antarctic sea ice over the 35-year period 1979–2013. *Ann. Glaciol.*, **56**, 18–28, doi:10.3189/2015AoG69A909.

Screen, J. A., and I. Simmonds, 2010: The central role of diminishing sea ice in recent Arctic temperature amplification. *Nature*, **464**, 1334–1337, doi:10.1038/nature09051.

——, and ——, 2013a: Exploring links between Arctic amplification and mid-latitude weather. *Geophys. Res. Lett.*, **40**, 959–964, doi:10.1002/grl.50174.

——, and ——, 2013b: Caution needed when linking weather extremes to amplified planetary waves. *Proc. Natl. Acad. Sci. USA*, **110**, E2327, doi:10.1073/pnas.1304867110.

——, and ——, 2014: Amplified mid-latitude planetary waves favour particular regional weather extremes. *Nat. Climate Change*, **4**, 704–709, doi:10.1038/nclimate2271.

——, and F. Francis, 2016: Contribution of sea-ice loss to Arctic amplification is regulated by Pacific Ocean decadal variability. *Nat. Climate Change*, **6**, 856–860, doi:10.1038/nclimate3011.

Simmonds, I., and P. D. Govekar, 2014: What are the physical links between Arctic sea ice loss and Eurasian winter climate? *Environ. Res. Lett.*, **9**, 101003, doi:10.1088/1748-9326/9/10/101003.

Tang, Q., X. Zhang, X. Yang, and J. A. Francis, 2013: Cold winter extremes in northern continents linked to Arctic sea ice loss. *Environ. Res. Lett.*, **8**, 014036, doi:10.1088/1748-9326/8/1/014036.

Tibaldi, S., and F. Molteni, 1990: On the operational predictability of blocking. *Tellus*, **42A**, 343–365, doi:10.1034/j.1600-0870.1990.t01-2-00003.x.

Vihma, T., 2014: Effects of Arctic sea ice decline on weather and climate. *Surv. Geophys.*, **35**, 1175–1214, doi:10.1007/s10712-014-9284-0.

Walsh, J. E., 2014: Intensified warming of the Arctic: Causes and impacts on middle latitudes. *Global Planet. Change*, **117**, 52–63, doi:10.1016/j.gloplacha.2014.03.003.

Yao, Y., and D. Luo, 2014: Relationship between zonal position of the North Atlantic Oscillation and Euro-Atlantic blocking events and its possible effect on the weather over Europe. *Sci. China Earth Sci.*, **57**, 2626–2638, doi:10.1007/s11430-014-4949-6.

Yu, Y., R. Ren, and M. Cai, 2015a: Dynamic linkage between cold air outbreaks and intensity variations of the meridional mass circulation. *J. Atmos. Sci.*, **72**, 3214–3230, doi:10.1175/JAS-D-14-0390.1.

——, ——, and ——, 2015b: Comparison of the mass circulation and AO indices as indicators of cold air outbreaks in northern winter. *Geophys. Res. Lett.*, **42**, 2442–2448, doi:10.1002/2015GL063676.

Zhang, Y.-C., W. B. Rossow, and A. A. Lacis, 1995: Calculation of surface and top of atmosphere radiative fluxes from physical quantities based on ISCCP data sets: 1. Methods and sensitivity to input data uncertainties. *J. Geophys. Res.*, **100**, 1149–1165, doi:10.1029/94JD02747.